Stability and collapse of rapidly rotating, supramassive neutron stars: 3D simulations in general relativity

Masaru Shibata
Department of Physics, University of Illinois at Urbana-Champaign, Urbana, Illinois 61801
and Department of Earth and Space Science, Graduate School of Science, Osaka University, Toyonaka, Osaka 560-0043, Japan

Thomas W. Baumgarte
Department of Physics, University of Illinois at Urbana-Champaign, Urbana, Illinois 61801

Stuart L. Shapiro
Department of Physics, University of Illinois at Urbana-Champaign, Urbana, Illinois 61801
and Department of Astronomy and NCSA, University of Illinois at Urbana-Champaign, Urbana, Illinois 61801
(Received 25 June 1999; published 26 January 2000)

We perform 3D numerical simulations in full general relativity to study the stability of rapidly rotating, supramassive neutron stars at the mass-shedding limit to dynamical collapse. We adopt an adiabatic equation of state with $\Gamma=2$ and focus on uniformly rotating stars. We find that the onset of dynamical instability along mass-shedding sequences nearly coincides with the onset of secular instability. Unstable stars collapse to rotating black holes within about one rotation period. We also study the collapse of stable stars which have been destabilized by pressure depletion (e.g., via a phase transition) or mass accretion. In no case do we find evidence for the formation of massive disks or any ejecta around the newly formed Kerr black holes, even though the progenitors are rapidly rotating.

PACS number(s): 04.25.Dm, 04.30.−w, 04.40.Dg

I. INTRODUCTION

Neutron stars found in nature are rotating. Rotation can support stars with higher mass than the maximum static limit, producing ''supramassive'' stars, as defined and calculated by Cook, Shapiro and Teukolsky [1,2]. Such supramassive stars can be created when neutron stars accrete gas from a normal binary companion. This scenario can also lead to ''recycled'' pulsars (see [3] for model calculations in general relativity). Alternatively, supramassive stars can be produced in the merger of binary neutron stars ([4] for discussions and references).

Pulsars are believed to be uniformly rotating. Eventually, viscosity will drive any equilibrium star to uniform rotation. Uniformly rotating configurations with sufficient angular momentum will be driven to the mass-shedding limit (at which the star's equator rotates with the Kepler frequency, so that any further spin-up would disrupt the star [3]). Supramassive neutron stars at the mass-shedding limit are the subject of this paper.

The dynamical stability of rotating neutron stars, including supramassive configurations, against radial perturbations, as well as the final fate of unstable stars undergoing collapse, has not been established definitively.

Along a sequence of nonrotating, spherical stars, parametrized by central density, the maximum mass configuration defines a critical density above which the stars are unstable to radial oscillations: stars on the high density, unstable branch collapse to black holes on dynamical time scales [5–7].

Establishing the onset of instability for rotating stars is more complicated. Chandrasekhar and Friedman [8] and Schutz [9] developed a formalism to identify points of *dynamical* instability to axisymmetric perturbations along sequences of rotating stars. In their formalism, however, a complicated functional for a set of trial functions has to be evaluated. Probably because of the complexity of their methods, explicit calculations have never been performed. Friedman, Ipser and Sorkin [10] showed that for uniformly rotating stars the onset of *secular* instability can be located quite easily by applying turning-point methods along sequences of constant angular momentum. This method has been applied to find points of secular instability in numerical models of uniformly rotating neutron stars [1,2,11].

Turning point methods along such sequences can only identify the point of secular, and not dynamical instability, since one is comparing neighboring, uniformly rotating configurations with the same angular momentum. Maintaining uniform rotation during perturbations tacitly assumes high viscosity. In reality, the star will preserve circulation as well as angular momentum in a dynamical perturbation, and not uniform rotation. It is thus possible that a secularly unstable star may be dynamically stable: for sufficiently small viscosity, the star may change to a differentially rotating, stable configuration instead of collapsing to a black hole. Ultimately, the presence of viscosity will bring the star back into rigid rotation, driving the star to an unstable state. A secular instability evolves on a dissipative, viscous time scale, while a dynamical instability evolves on a collapse (free-fall) time scale. Friedman, Ipser and Sorkin [10] showed that along a sequence of uniformly rotating stars, a secular instability always occurs *before* a dynamical instability (implying that all secularly stable stars are also dynamically stable).

For spherical stars, the onset of secular and dynamical instability coincides (since for a nonrotating star a radial perturbation conserves both circulation and uniform rotation).

This suggests that for uniformly rotating stars for which the rotational kinetic energy T is typically a small fraction of the gravitational energy W, the onset of dynamical instability is close to the onset of secular instability. One goal of this paper is to test this hypothesis and to identify the onset of dynamical instability in rotating stars.

We also follow the nonlinear growth of the radial instability and determine the final fate of unstable configurations. Nonrotating neutron stars collapse to black holes, but rotating stars could also form black holes surrounded by massive disks. Also, if J/M_g^2 exceeds the Kerr limit of unity (where J is the angular momentum and M_g the total mass-energy or gravitational mass of the progenitor star), not all of the matter can collapse directly to a black hole. As pointed out recently, such a system could be the central source of γ-ray bursts [12].

Numerical hydrodynamic simulations in full general relativity (GR) provide the best approach to understanding the collapse of rotating neutron stars. Two groups [13,14] included rotation in axisymmetric, relativistic hydrodynamic codes to study the collapse of rotating massive stars to black holes. The collapse and fate of unstable rotating neutron stars, however, has never been simulated before. Probably this is because numerical methods for constructing initial data describing rapidly rotating neutron stars, as well as numerical tools, techniques and sufficient computational resources have only become available recently. Over the last few years, robust numerical techniques for constructing equilibrium models of rotating neutron stars in full GR have been established [1,2,11,15–17]. More recently, methods for the numerical evolution of 3D gravitational fields have been developed (see, e.g., [18–24]). In a previous paper [25], Shibata presented a wide variety of numerical results of test problems for his 3D hydrodynamic GR code and demonstrated that simulations for many interesting problems are now feasible.

In this paper, we perform simulations in full GR for rapidly rotating neutron stars. This study is a by-product of our long-term effort to build robust, fully relativistic, hydrodynamic evolution codes in 3D. We adopt rigidly rotating supramassive neutron stars at mass-shedding as initial data. By exploring rotating stars at mass-shedding, we can clarify the effect of rotation most efficiently. Such stars are also the plausible outcome of pulsar recycling and binary coalescence. Following Ref. [25], we prepare equilibrium states for such stars using an approximation in which the spatial metric is assumed to be conformally flat. We then perform numerical simulations to investigate the dynamical stability of the rapidly rotating neutron stars against collapse and to determine the final fate of the unstable neutron stars. We believe that this is the first 3D simulation of the dynamical collapse of a rotating neutron star in full GR.

In Newtonian physics, stars with sufficient rotation ($T/|W| \gtrsim 0.27$) are dynamically unstable to bar formation [26–28]. Since $T/|W|$ increases approximately with R^{-1} as a star collapses, radial collapse may drive the dynamical growth of nonaxisymmetric bars. To allow for this possibility, a numerical simulation must be performed in 3D, not in axisymmetry.

In Sec. II, we briefly describe our formulation, initial data, and spatial gauge conditions. In Sec. III, we present numerical results. First, we study the dynamical stability of supramassive rotating neutron stars at the mass-shedding limit. We then study the final products of the unstable neutron stars adopting three kinds of initial conditions: In the first case, we choose a marginally stable neutron star and slightly reduce the pressure for destabilization as the initial condition. In the second case, we prepare a stable star, and then reduce a large fraction of the pressure suddenly. While we are primarily interested in computational consequences, this scenario may provide a model for sudden phase transitions inside neutron stars (see, e.g., [29,30] and references therein). In the third case, we prepare a stable star and add more mass near the surface to induce collapse. In all the cases, we find that the final products are black holes without surrounding massive disks, which we can readily explain. In Sec. IV we provide a summary. Throughout this paper, we adopt the units $G=c=M_\odot=1$ where G, c and $M_\odot$ denote the gravitational constant, speed of light and solar mass, respectively. We use Cartesian coordinates $x^k=(x,y,z)$ as the spatial coordinate with $r=\sqrt{x^2+y^2+z^2}$; t denotes coordinate time.

II. METHODS

A. Summary of formulation

We perform numerical simulations using the same formulation as in [25], to which the reader may refer for details and basic equations. The fundamental variables used in this paper are

ρ: rest mass density,

ε: specific internal energy,

P: pressure,

u^μ: four velocity,

α: lapse function,

β^k: shift vector,

γ_{ij}: metric in 3D spatial hypersurface,

$$\gamma = e^{12\phi} = \det(\gamma_{ij}),$$

$$\tilde{\gamma}_{ij} = e^{-4\phi}\gamma_{ij},$$

K_{ij}: extrinsic curvature.

General relativistic hydrodynamic equations are solved using the van Leer scheme for the advection terms [31]. Geometric variables (together with three auxiliary functions F_i and the trace of the extrinsic curvature) are evolved with a free evolution code. The boundary conditions for geometric variables are the same as those adopted in [25]. Violations of the Hamiltonian constraint and conservation of mass and angular momentum are monitored as code checks. Several test calculations, including spherical collapse of dust, stability of

spherical neutron stars, and the evolution of rotating neutron stars as well as corotating binary systems have been described in [25]. Black holes that form during the late phase of the collapse are located with an apparent horizon finder as described in [32].

We also define a density $\rho_*(=\rho\alpha u^0 e^{6\phi})$ from which the total rest mass of the system can be integrated as

$$M_* = \int d^3x \rho_* . \tag{2.1}$$

We perform the simulations assuming π-rotation symmetry around the z-axis as well as a reflection symmetry with respect to the $z=0$ plane and using a fixed uniform grid with the typical size $153\times77\times77$ in $x-y-z$. We have also performed test simulations with different grid resolutions to check that the results do not change significantly.

The slicing and spatial gauge conditions we use in this paper are basically the same as those adopted in [25]; i.e., we impose an ''approximate'' maximal slice condition ($K_k{}^k \simeq 0$) and an ''approximate'' minimum distortion gauge condition [$\tilde{D}_i(\partial_t \tilde{\gamma}^{ij}) \simeq 0$ where $\tilde{D}_i$ is the covariant derivative with respect to $\tilde{\gamma}_{ij}$]. However, for the case when a rotating star collapses to a black hole, we slightly modify the spatial gauge condition in order to improve the spatial resolution around the black hole. The method of the modification is described in Sec. II. C.

B. Initial conditions for rotating neutron stars

As initial conditions, we adopt rapidly and rigidly rotating supramassive neutron stars in (approximately) equilibrium states. The approximate equilibrium states are obtained by choosing a conformally flat spatial metric, i.e., assuming $\gamma_{ij}=e^{4\phi}\delta_{ij}$. This approach is computationally convenient and, as illustrated in [33], provides an excellent approximation to exact axisymmetric equilibrium configurations.

Throughout this paper, we assume a Γ-law equation of state in the form

$$P=(\Gamma-1)\rho\varepsilon, \tag{2.2}$$

where Γ is the adiabatic constant. For hydrostatic problems, the equation of state can be rewritten in the polytropic form

$$P=K\rho^{\Gamma}, \quad \Gamma=1+\frac{1}{n}, \tag{2.3}$$

where K is the polytropic constant and n the polytropic index. We adopt $\Gamma=2$ $(n=1)$ as a reasonable qualitative approximation to realistic (moderately stiff) cold, nuclear equations of state.

Physical units enter the problem only through the polytropic constant K, which can be chosen arbitrarily or else completely scaled out of the problem. We often quote values for $K=200/\pi$, for which in our units $(G=c=M_\odot=1)$ the radius is $R=(\pi K/2)^{1/2}=10$ in the Newtonian limit; corresponding to $R\sim15$ km. Since $K^{n/2}$ has units of length, dimensionless variables can be constructed as

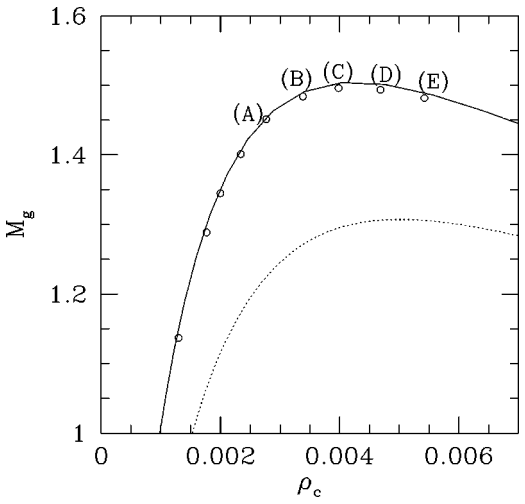

FIG. 1. The gravitational mass M_g as a function of the central density ρ_c for rotating stars with $\Gamma=2$ and $K=200/\pi$. The solid and dashed lines denote exact solutions for sequences of rotating stars at the mass-shedding limit and spherical stars. The open circles denote the sequence of rotating stars at the mass-shedding limit as obtained from the conformal flatness approximation. The configurations that we adopt as initial data for dynamical evolution calculations in this paper are marked with (A)–(E).

$$\bar{M}_* = M_* K^{-n/2}, \quad \bar{M}_g = M_g K^{-n/2}, \quad \bar{R} = R K^{-n/2},$$
$$\bar{J} = J K^{-n}, \quad \bar{\mathrm{P}} = \mathrm{P} K^{-n/2}, \quad \bar{\rho} = \rho K^{n}, \tag{2.4}$$

where P denotes rotational period. All results can be scaled for arbitrary K using Eqs. (2.4).

For the construction of the (approximate) equilibrium states as initial data, we adopt a grid in which the semi-major axes of the stars, along the x and y axes, are covered with 40 grid points. For rotating stars at mass-shedding near the maximum mass, the semi-minor (rotation) axis along the z axis is covered with 23 or 24 grid points.

In Fig. 1, we show the relation between the gravitational mass M_g and the central density ρ_c for the neutron stars. The solid and dotted lines denote the relations for spherical neutron stars and stars rotating at the mass-shedding limit, constructed from the exact stationary matter and field equations. The open circles denote the approximate equilibrium states at the mass-shedding limit obtained using the conformal flatness approximation. We find that at $\rho_c=\rho_{\max}$ where $0.0040 \lesssim \rho_{\max} \lesssim 0.0045$, M_g takes its maximum value. For stars with stiff equations of state the numerical results in Ref. [2] show that the central density at the onset of secular instability (which hereafter we refer to as $\rho_{\rm crit}$) is very close to $\rho_{\max}$ (see, e.g., Fig. 4 of [2]). We therefore consider stars with $\rho_c \geqslant \rho_{\max}(\simeq\rho_{\rm crit})$ as candidates for dynamically unstable stars.

C. Spatial gauge condition

When no black hole is formed, we adopt the approximate minimum distortion (AMD) gauge condition as our spatial gauge condition. However, as pointed out in previous papers

[24,25], during the black hole formation (i.e., for an infalling radial velocity field), the expansion of the shift vector $\partial_i \beta^i$ and the time derivative of ϕ becomes positive using this gauge condition together with maximal slicing. Accordingly, the coordinates diverge outward and the resolution around the black hole forming region becomes worse and worse during the collapse. This undesirable property motivates us to modify the AMD gauge condition when we treat black hole formation. Specifically, we modify the AMD shift vector according to

$$\beta^i = \beta^i_{\rm AMD} - f(t,r)\frac{x^i}{r+\epsilon}\beta^{r'}_{\rm AMD}. \tag{2.5}$$

Here $\beta^i_{\rm AMD}$ denotes the shift vector in the AMD gauge condition, $\beta^{r'}_{\rm AMD} \equiv x^k \beta^k_{\rm AMD}/(r+\epsilon)$, ϵ is a small constant much less than the grid spacing, and $f(t,r)$ is a function chosen as

$$f(t,r) = f_0(t)\frac{1}{1+(r/M_{g,0})^4}, \tag{2.6}$$

where $M_{g,0}$ denotes the gravitational mass of a system at $t=0$. We determine $f_0(t)$ from $\phi_0 = \phi(r=0)$. Taking into account the fact that the resolution around $r=0$ deteriorates when ϕ_0 becomes large, we choose f_0 according to

$$f_0(t) = \begin{cases} 1 & \text{for } \phi_0 \geqslant 0.8, \\ 2.5\phi_0 - 1 & \text{for } 0.4 \leqslant \phi_0 \leqslant 0.8 \quad \text{type I}, \\ 0 & \text{for } \phi_0 < 0.4, \end{cases} \tag{2.7}$$

or

$$f_0(t) = \begin{cases} 1 & \text{for } \phi_0 \geqslant 0.6, \\ 5\phi_0 - 2 & \text{for } 0.4 \leqslant \phi_0 \leqslant 0.6 \quad \text{type II}, \\ 0 & \text{for } \phi_0 < 0.4. \end{cases} \tag{2.8}$$

Note that for spherical collapse with $f_0 = 1$, $\partial_i \beta^i \sim 0$ at $r=0$ in both cases. In general, we find numerically that $\partial_i \beta^i$ is small near the origin, where the collapse proceeds nearly spherically. In the following, we refer to the modified gauge conditions of f_0 defined by Eqs. (2.7) and (2.8) as type I and II, respectively. We employ them whenever a rotating neutron star collapses to a black hole.

III. NUMERICAL RESULTS

A. Dynamical stability

We investigate the stability of supramassive rotating neutron stars at mass-shedding limits against gravitational collapse. We adopt the stars marked with (A), (B), (C), (D), and (E) in Fig. 1 as initial conditions for our numerical experiments. The physical properties of these stars are summarized in Table I. In this numerical experiment, we adopt two initial conditions for each model. In one case, we use the (approximate) equilibrium states of rotating neutron stars without any perturbation and in the other case, we uniformly reduce the pressure by 1% (by decreasing K; i.e., $\Delta K/K = 1\%$ where ΔK denotes the depletion factor of K [35]).

TABLE I. The list of the central density ρ_c, total rest mass M_*, gravitational mass M_g, angular momentum in units of M_g^2 (J/M_g^2), T/W, rotation period P, and coordinate length of the semi-major axis R_e for rotating neutron stars at mass-shedding limits in the conformal flat approximation. The gauge invariant definition of T/W is the same as that in Ref. [1]. The units of mass, length and time are $M_\odot$, 1.477 km, and 4.927 μsec, respectively.

$\rho_c(10^{-3})$	M_*	M_g	J/M_g^2	T/W	P	R_e	Model
2.77	1.580	1.452	0.598	0.087	163	8.064	(A)
3.38	1.628	1.484	0.586	0.085	148	7.820	(B)
3.98	1.646	1.496	0.574	0.083	137	7.365	(C)
4.68	1.645	1.494	0.563	0.080	127	6.934	(D)
5.43	1.630	1.481	0.553	0.078	120	6.566	(E)

In Fig. 2, we show ρ and α at $r=0$ [34] as a function of $t/$P where P is the rotation period of each rotating star. We find that when $\rho_c < \rho_{\rm crit}$ [i.e., stars (A), (B) and (C)], the rotating stars oscillate independent of the initial perturbations. Hence, these stars are stable against gravitational collapse. We note that we find small amplitude oscillations even when we do not reduce the pressure initially. This is caused by small deviations of the initial data from true equilibrium states, both because of the conformal flatness approximation and because of numerical truncation error.

We expect the oscillation frequencies in Fig. 2 to be the fundamental quasi-radial oscillation of these rotating stars. The oscillation periods increase with the central density. At the marginally stable point of secular stability ($\rho_c = \rho_{\rm crit}$), the period becomes infinite.

Star (D) does not collapse either and instead oscillates for $\Delta K = 0$. However, it collapses for $\Delta K/K = 1\%$. This indi-

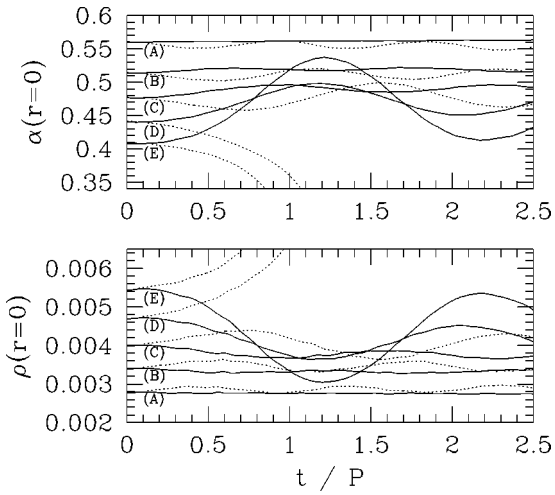

FIG. 2. α and ρ at $r=0$ as a function of $t/$P in the evolution of stars (A)–(E). The solid and dotted lines denote the results for $\Delta K = 0$ and $\Delta K/K = 1\%$, respectively.

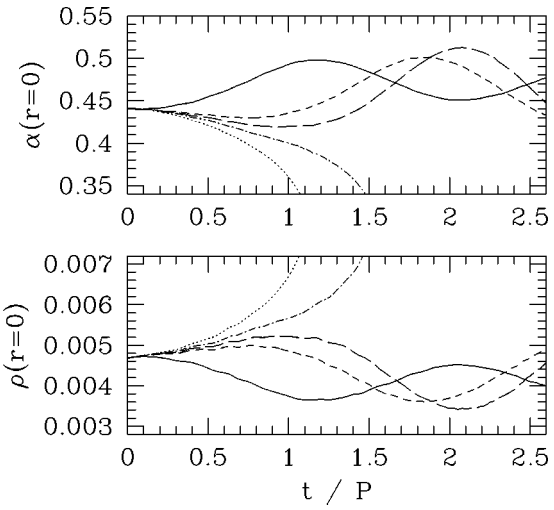

FIG. 3. α and ρ at $r=0$ as a function of t/P during the evolution of star (D) for various $\Delta K/K$. The solid, dashed, long dashed, dotted-dashed, and dotted lines denote the results for $\Delta K/K=0$, 0.7%, 0.8%, 0.9%, and 1%.

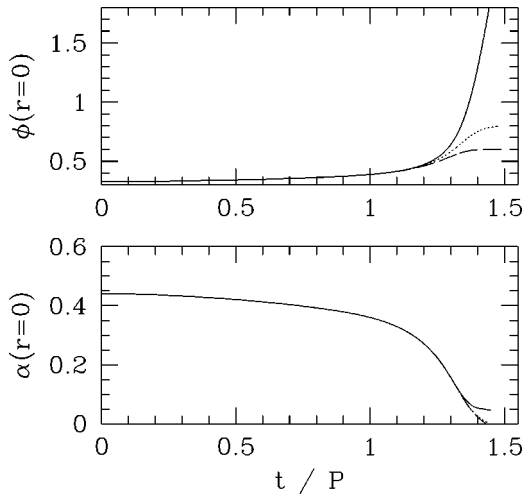

FIG. 4. ϕ and α at $r=0$ as a function of t/P during the collapse of star (D) with $\Delta K/K=1\%$ for the AMD gauge (the solid line), the modified gauge of type I (the dotted line) and of type II (the dashed line), respectively.

cates that star (D) is located near the onset point of dynamical stability. It is found that the oscillation amplitude for the case $\Delta K=0$ is very large compared with those for (A)–(C). This could be caused by two effects: (i) star (D) is near the onset of dynamical instability and hence a small deviation from true equilibrium can induce large perturbations; (ii) the conformal flatness approximation results in larger deviations from true equilibrium for more relativistic configurations, which causes a larger initial perturbation. Apparently, the deviation caused by the numerical truncation error and/or the conformal flatness approximation stabilizes the configuration, and for $\Delta K=0$ the star oscillates with an average value of the central density [$\rho(r=0)\simeq 0.004$] slightly smaller than the initial value $\rho_c\simeq 0.0047$. This suggests that star (D) with $\Delta K=0$ is a perturbed state of a true equilibrium star of $\rho_c \simeq 0.004\sim\rho_{\mathrm{crit}}$. The results for star (E) are similar to, but more pronounced than those for star (D), suggesting that the initial configuration (E) may also be a perturbation of a stable star with $\rho_c\simeq 0.004\sim\rho_{\mathrm{crit}}$.

To determine the onset of dynamical instability more sharply, we perform further simulations adopting $\Delta K/K=0.7\%$, 0.8%, and 0.9% for star (D). In Fig. 3, we show ρ and α at $r=0$ as a function of t/P for star (D) for the various initial depletion factors. We find that for $\Delta K/K\leqslant 0.8\%$, the stars behave similarly to $\Delta K=0$; i.e., the stars simply oscillate with the average density $\simeq\rho_{\mathrm{crit}}$. For $\Delta K/K\geqslant 0.9\%$, however, the stars quickly collapse to a black hole. We do not find any examples in which the stars oscillate with average densities larger than $0.0045\gtrsim\rho_{\mathrm{crit}}$. This indicates that equilibrium stars with $\rho_c\gtrsim\rho_{\mathrm{crit}}$ are dynamically unstable. Although we cannot specify the onset of dynamical instability with arbitrary precision, our present results indicate that it nearly coincides with the onset of secular instability.

B. Final outcome of unstable collapse

To study the final outcome of the gravitational collapse of rapidly rotating neutron stars, we perform a number of numerical experiments for several different initial conditions.

First, we evolve star (D) with $\Delta K/K=1\%$ for different spatial gauge conditions. In Fig. 4, we show ϕ and α at $r=0$ as a function of time for the AMD gauge (solid line), the modified gauge of type I (dotted line) and type II (dashed line). As stated in Sec. II B, $\phi(r=0)$ increases quickly during the gravitational collapse for the AMD gauge. In this case, $\alpha(r=0)$ stops decreasing in the late phase of the collapse where $\phi(r=0)\gtrsim 1$, which is a numerical artifact. This is probably caused by the insufficient resolution around the black hole forming region. For the modified gauge conditions, $\alpha(r=0)$ smoothly approaches zero. We note that $\alpha(r=0)$ ought to be independent of the spatial gauge condition, so that the deviation of the AMD results from the modified gauge condition results are a numerical artifact. This shows that the results for $t/\mathrm{P}\gtrsim 1.4$ computed in the AMD gauge condition is unreliable and indicates that the modifi-

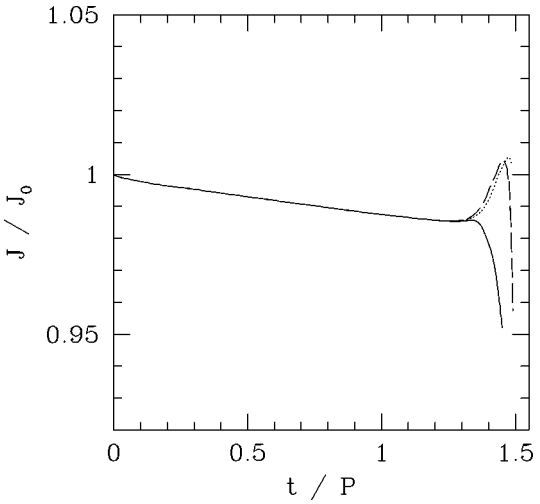

FIG. 5. Same as Fig. 4, but for the angular momentum J/J_0 as a function of t/P. Here, J_0 is the angular momentum of the system at $t=0$.

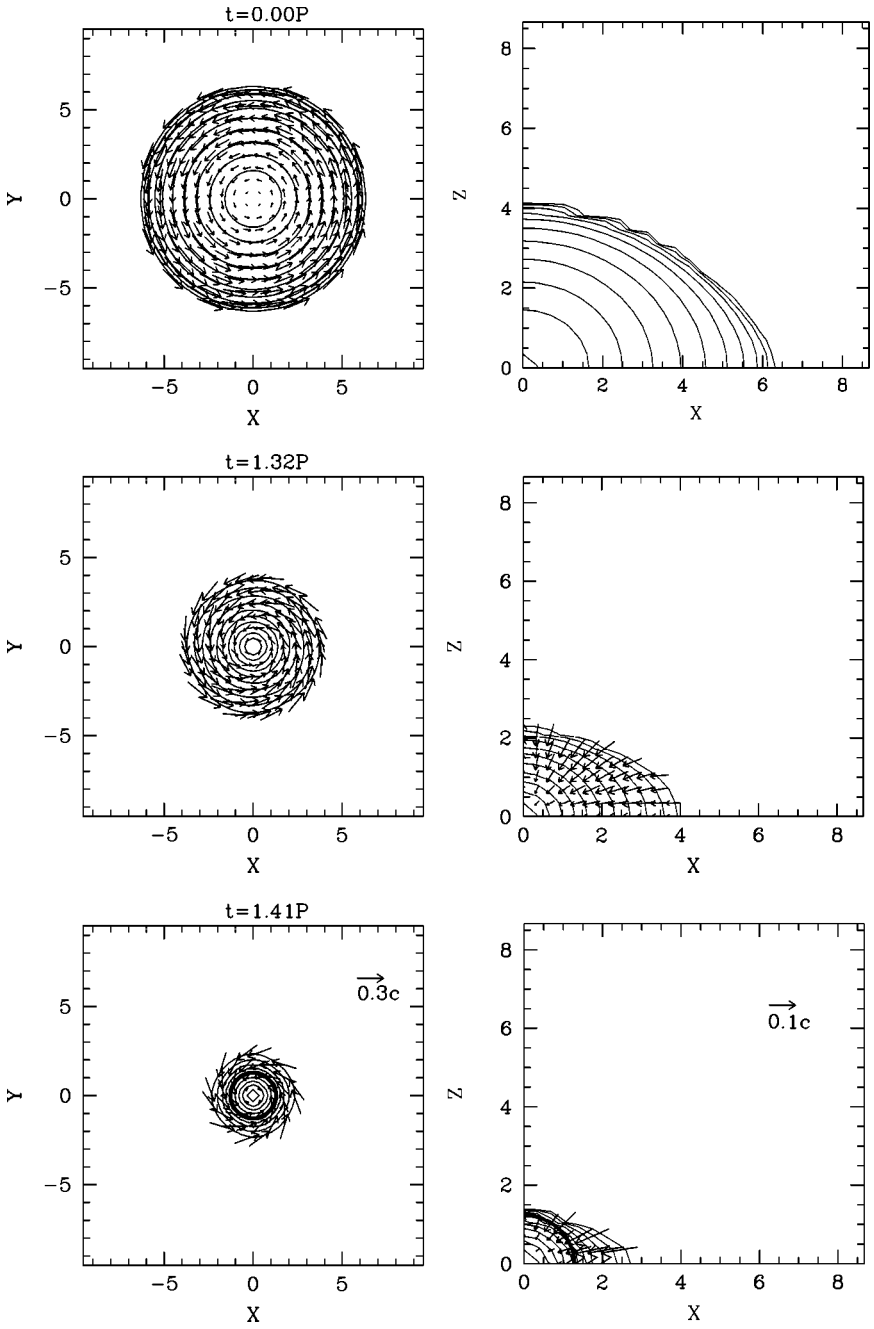

FIG. 6. Snapshots of density contours for ρ_* and the velocity flow for (v^x, v^y) in the equatorial plane (left) and in the $y=0$ plane (right) for the collapse of star (D) with $\Delta K/K=1\%$ (evolved with type I modified AMD gauge). The contour lines are drawn for $\rho_*/\rho_{*\ c}=10^{-0.3j}$ for $j=0,1,2,\ldots,10$ where $\rho_{*\ c}$ is 0.034, 0.64, and 2.04 for the three different times. The lengths of arrows are normalized to $0.3c$ (left) and $0.1c$ (right). The thick solid lines denote the location of the apparent horizon.

cation of the AMD gauge condition is an appropriate strategy to overcome the deterioration of the resolution in the late phase of the collapse.

In Fig. 5, we show the time variation of the total angular momentum of the system. Since the evolving system is nearly axisymmetric, the angular momentum should be nearly conserved. In all the three cases, however, the angular momentum slowly decreases in the early phase, which is caused by numerical dissipation at the stellar surface. As the collapsing star approaches a black hole, the angular momentum changes quickly because the resolution becomes increasingly worse. In the AMD gauge case, the error amounts to $\gtrsim 5\%$, while in the modified gauge cases, it is $\sim 1.5\%$ at the time when apparent horizon is found at $t\sim 1.4$P (see Fig. 6). This is further evidence that the modified gauge conditions are better suited for simulations of black hole formation.

It should be noted that even with the modified gauge conditions, the resolution becomes too poor to perform accurate simulations for times exceeding $t/\mathrm{P}\gtrsim 1.5$. This is because the metric $\tilde{\gamma}_{ij}$ becomes very spiky around the apparent horizon (i.e., because of horizon throat stretching). To perform simulations for times much later than horizon formation special

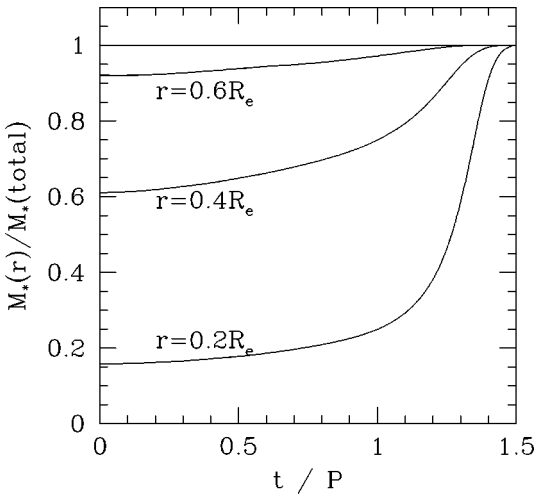

FIG. 7. Fraction of the rest mass inside a coordinate radius r as a function of t/P for star (D) with $\Delta K/K=1\%$ (evolved with type I modified AMD gauge). R_e denotes the initial coordinate length of the semi-major axis.

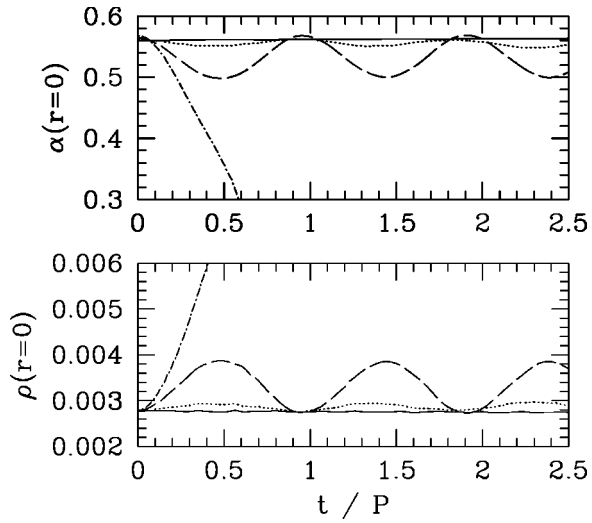

FIG. 8. α and ρ at $r=0$ as a function of t/P for star (A) of various initial pressure depletion factors $\Delta K/K$. The solid, dotted, dashed, and dotted-dashed lines denote the cases where $\Delta K/K=0\%$, 1%, 5%, and 10%, respectively.

computational tools are necessary, probably including apparent horizon boundary conditions [36].

In Fig. 6, we show snapshots of density contour lines for the density ρ_* and the velocity field for $v^i(=u^i/u^0)$ in the equatorial and $y=0$ planes. The results are obtained in the modified gauge condition of type I. It is found that after about 1.4 orbital periods almost all the matter has collapsed to a black hole. In Fig. 7, we show the fraction of the rest mass inside a coordinate radius r, defined as

$$\frac{M_*(r)}{M_*}=\frac{1}{M_*}\int_{|x^i|<r} d^3x\rho_*\,. \tag{3.1}$$

R_e denotes the coordinate axial length in the equatorial plane at $t=0$ (see Table I). Note that at $t\sim 1.4$P, the apparent horizon is located at $r\simeq 0.2R_e$. Thus, almost all the matter (more than 99%) has been absorbed by the black hole by that time. Although Fig. 6 shows that a small fraction of the matter has not yet been swallowed by the black hole, the matter which stays inside $r\lesssim R_e\sim 5M_g$ will ultimately have to fall in. This is, because the radius of the innermost stable circular orbit (ISCO) is $R^{\rm SS}_{\rm ISCO}\sim 5M_g$ for a (nonrotating) Schwarzschild black hole in our gauge. The collapse of rotating neutron stars with $J/M_g^2\sim 0.6<1$ leads to moderately rotating Kerr black holes, for which $R^{\rm SS}_{\rm ISCO}$ is an adequate approximation to the ISCO. This fact already suggests that no disk will form around the black hole.

The same reason also suggests why no massive disk forms during the collapse: the equatorial radius R_e is initially less than $5M_g$, and hence inside the radius which will become the ISCO of the final black hole.

Next, we evolve the initial configuration (A) depleting the pressure by various amounts, which may provide a model for sudden phase transitions inside neutron stars [29,30]. In Fig. 8, we show ρ and α at $r=0$ as a function of time for $\Delta K/K=0$,1%, 5%, and 10% [35]. When the depletion factor is less than 5%, the star simply oscillates, but for $\Delta K/K=10\%$ the star collapses dynamically. Note that depleting the pressure by 10% is approximately equivalent to increasing the gravitational mass by 5% according to the scaling relation for the polytropic stars of $\Gamma=2$ [see Eq. (2.4)]. Since the gravitational mass for star (A) is about 3% less than the maximum allowed mass, it is quite reasonable that this star collapses. In the following two simulations, we focus on evolutions of star (A) with $\Delta K/K=10\%$.

In order to test if nonaxisymmetric (bar-mode) perturbations have enough time to grow appreciably during the gravitational collapse, we excite such a perturbation by modifying the initial density profile ρ_* according to [35]

$$\rho_*=(\rho_*)_0\left(1+0.3\frac{x^2-y^2}{R_e^2}\right), \tag{3.2}$$

where $(\rho_*)_0$ denotes the density profile of star (A) in the unperturbed state.

In Figs. 9 and 10, we show snapshots of density contour lines for ρ_* and the velocity field for v^i in the equatorial and $y=0$ planes for the above axisymmetric and nonaxisymmetric initial conditions. For these simulations we adopted the modified gauge condition of type II. In Fig. 11, we also show $M_*(r)/M_*$ as a function of time for these cases. We again find that irrespective of the initial perturbation, almost all the matter collapses into the black hole without any massive disk or ejecta around the black hole. Again, this is a consequence of the stars being sufficiently compact that almost all the matter ends up inside the ISCO of the final black hole. Note that the star with the nonaxisymmetric perturbation evolves very similarly to the unperturbed, axisymmetric star, showing that the dynamical collapse does not leave the nonaxisymmetric perturbation enough time to grow appreciably during the collapse. Again, this can be understood quite easily from the following heuristic (and Newtonian) argument. Star (A) has an initial equatorial radius of $R_e\sim 5.5M_g$, and

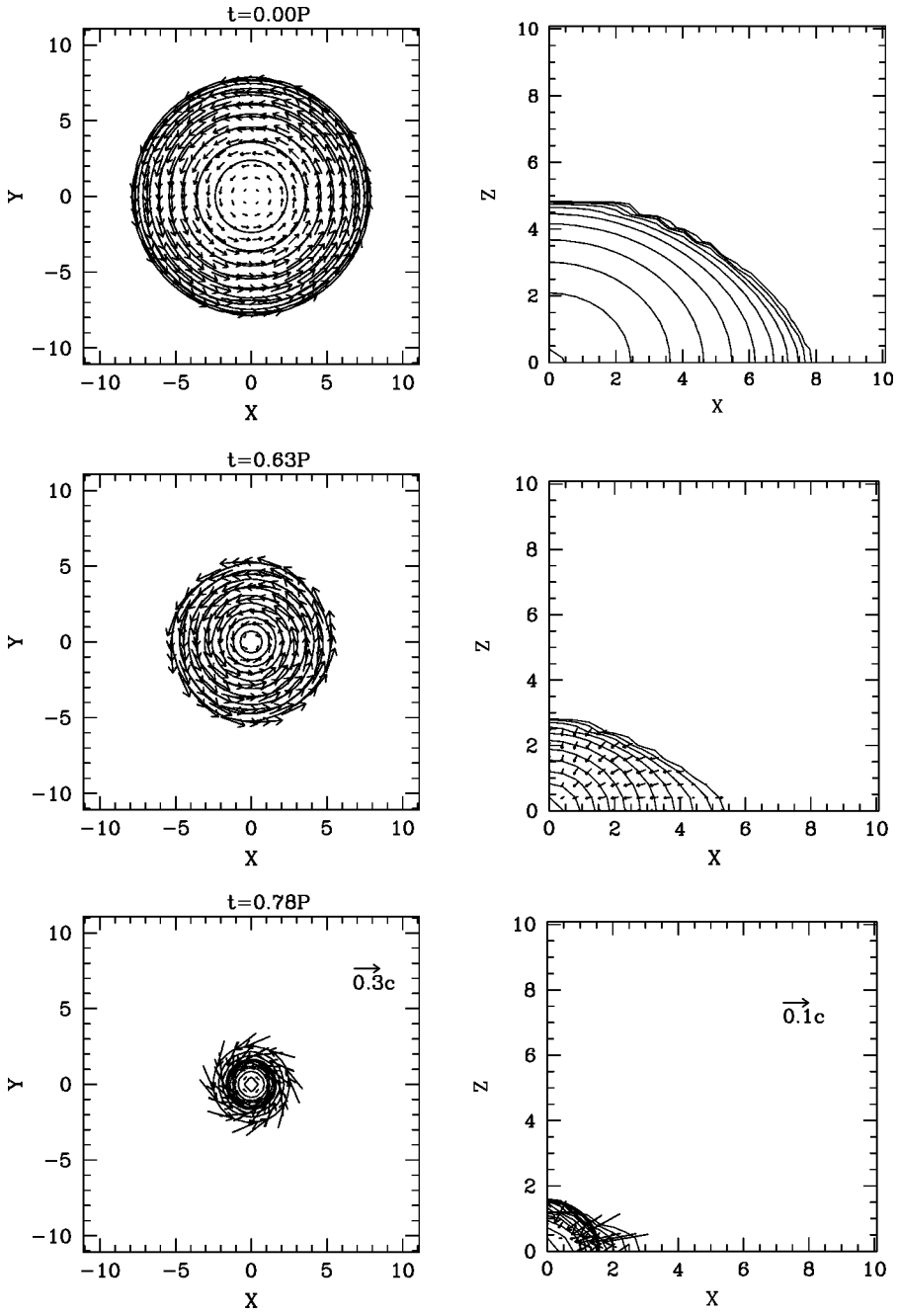

FIG. 9. Same as Fig. 6, but for star (A) with $\Delta K/K=10\%$. The contour lines are drawn for $\rho_*/\rho_{*\ c}=10^{-0.3j}$ for $j=0,1,2,\ldots,10$ where $\rho_{*\ c}$ is 0.012, 0.20, and 1.01 for the three different times.

can therefore shrink by less than a factor of 3 before a black hole forms. Its initial value of $T/|W|$ is about 0.09 (see Table I). Since $T/|W|$ scales approximately with R^{-1}, it can just barely reach the critical value $(T/|W|)_{\rm dyn}\sim 0.27$ for dynamical instability before a black hole forms. It is therefore not surprising that we do not find dynamically growing axisymmetric perturbations. Note that the star does reach the critical value for secular instability to bar formation [which may be as small as $(T/|W|)_{\rm sec}\sim 0.1$ for very compact configurations, see [37]], so that viscosity or emission of gravitational waves could drive the star unstable. However, this mode would grow on the corresponding dissipative time scale, which is much longer than the dynamical time scale of the collapse.

In order to make these statements about nonaxisymmetric growth more quantitative, we compare the quantities

$$2\frac{x_{\rm rms}-y_{\rm rms}}{x_{\rm rms}+y_{\rm rms}} \tag{3.3}$$

for the perturbed and unperturbed evolutions in Fig. 12. Here, $x^i_{\rm rms}$ denotes the mean square axial length defined as

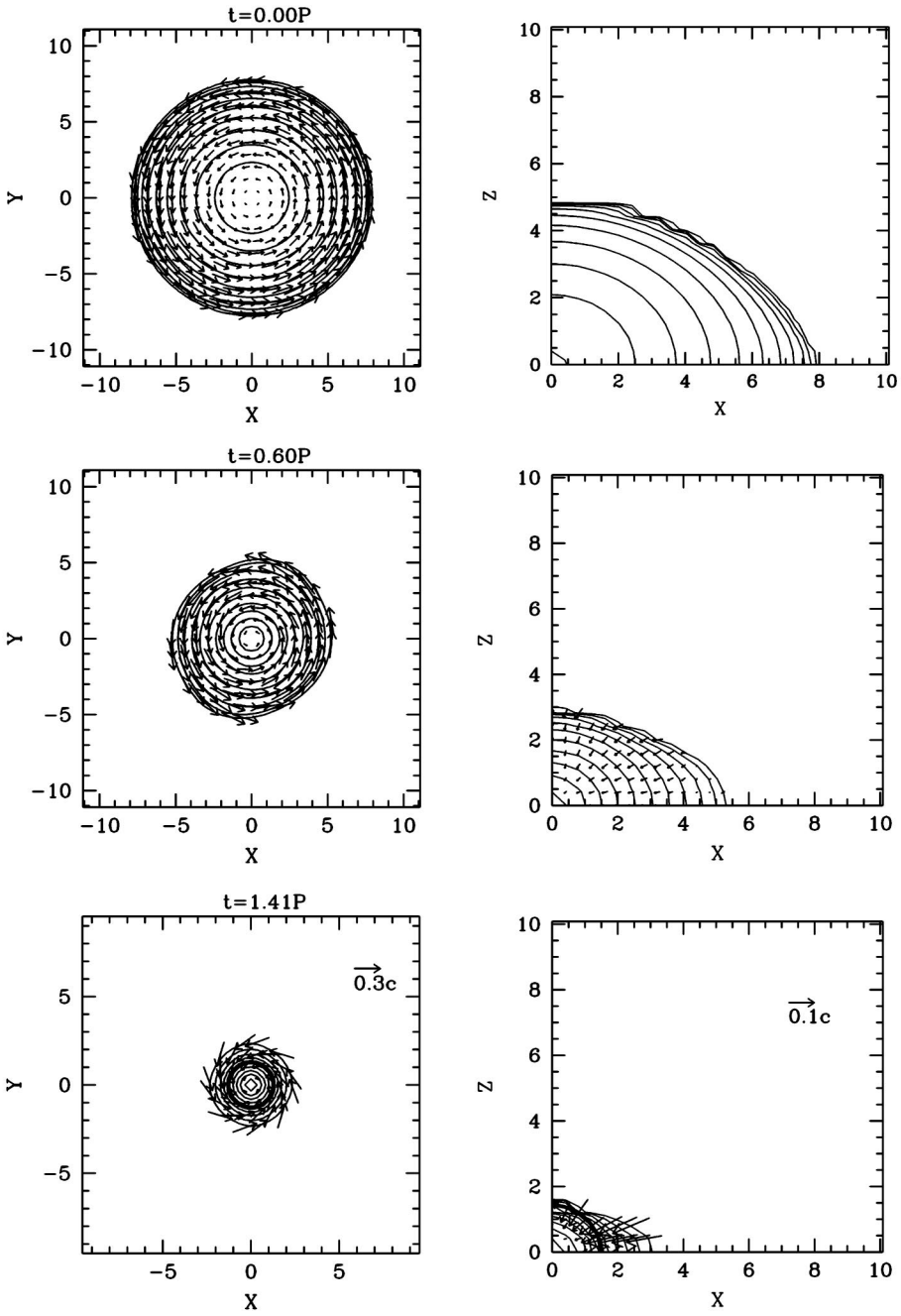

FIG. 10. Same as Fig. 6, but for star (A) with $\Delta K/K=10\%$ and the nonaxisymmetric perturbation (3.2). The contour lines are drawn for $\rho_*/\rho_{*\ c}=10^{-0.3j}$ for $j=0,1,2,\ldots,10$ where $\rho_{*\ c}$ is 0.012, 0.15, and 0.99 for the three different times.

$$x^i_{\rm rms}=\left[\frac{1}{M_*}\int d^3x\rho_*(x^i)^2\right]^{1/2}. \tag{3.4}$$

$$\rho_*=(\rho_*)_0\left(1+0.5\frac{r^2}{R_e^2}\right), \tag{3.5}$$

The figure shows very clearly that the axial ratio oscillates for the perturbed evolution, but does not grow on the dynamical timescale of the collapse.

Finally, we model a scenario in which a small amount of matter accretes onto a stable star resulting in destabilization of the star. As the stable star, we again adopt configuration (A) and to model the matter accretion we modify the initial density distribution according to [35]

with all the matter moving with the same initial angular velocity. Most of the enhancement is in the outer region, which mimics the effect of accretion. In this case, the total rest mass is about 9.5% larger than that of star (A), so that the mass is larger than the maximum allowed mass along the sequence of rotating neutron stars. The value of J/M_g^2 is nearly unchanged. Note that we do not reduce the pressure

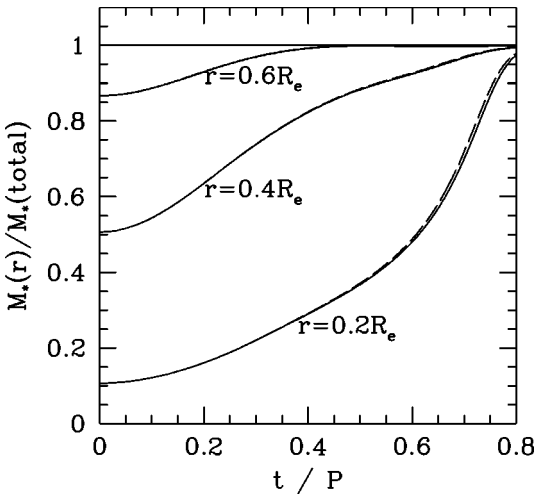

FIG. 11. Same as Fig. 7, but for star (A), $\Delta K/K=10\%$, with (solid line) and without (dashed line) the nonaxisymmetric perturbation (3.2).

for these simulations. We again evolve the star using the modified gauge condition of type II.

The star again evolves very similarly to those in the previous two cases. As an example, we show in Fig. 13 $M_*(r)/M_*$ as a function of time, which is similar to the results in Fig. 11. The apparent horizon forms at $t\simeq 0.89$P and $r\simeq 0.2R_e$. We again find that almost all the matter collapses into the black hole without forming a massive disk around the black hole.

IV. SUMMARY AND CONCLUSION

We perform fully relativistic, 3D hydrodynamic simulations of supramassive neutron stars rigidly rotating at the mass-shedding limit. We study the dynamical stability of such stars close to the onset of secular instability and follow the collapse to rotating black holes.

Our results suggest that the onset of dynamical, radial instability is indeed close to the onset of secular instability,

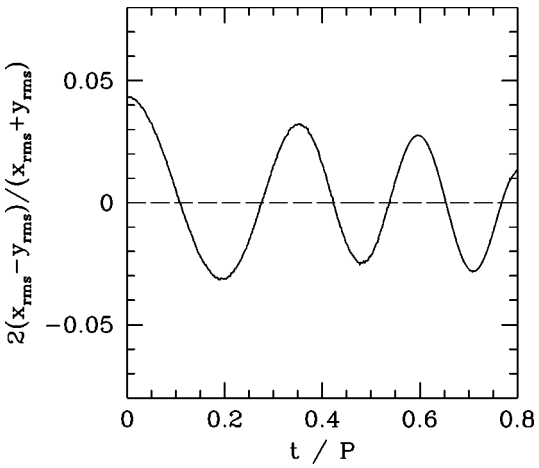

FIG. 12. Same as Fig. 11, but for the mean square axial length [see Eq. (3.3)]. The solid and dashed lines denote simulations with and without the nonaxisymmetric perturbation (3.2).

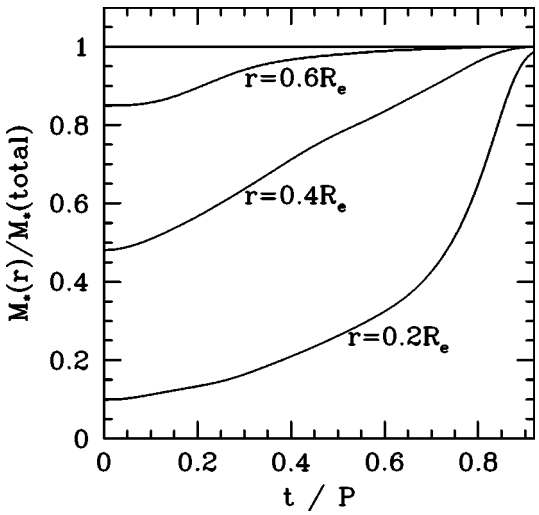

FIG. 13. Same as Fig. 7, but for collapse with the initial density profile (3.4) [mimicking star (A) driven into instability by accretion of additional matter].

as expected from the coincidence of the secular and dynamical instability in nonrotating, spherical stars.

In all our simulations, nearly all the matter is consumed by the nascent black hole by the time the calculation stops, and we do not find any evidence for a formation of a massive disk or any ejecta. Since we are considering maximally rotating neutron stars at the mass-shedding limit, and since the formation of a disk is even less likely for more slowly rotating stars, we conclude that such disks quite generally do not form during the collapse of unstable, uniformly rotating neutron stars. This also includes stars which are destabilized by pressure depletion (as, for example, by a nuclear phase transition), or by mass accretion.

We also find that during the collapse to a black hole, nonaxisymmetric perturbations do not have enough time to grow appreciably.

Both these findings can be understood quite easily from heuristic arguments. The initial equilibrium configurations are sufficiently compact, typically $R_e\lesssim 6M_g$, so that most of the matter already starts out inside the radius which will become the ISCO of the final black hole. Therefore it is very unlikely that a stable, massive disk would form. Also, the star can only contract by about a factor of three before a black hole forms. Hence $T/|W|$, which approximately scales with R^{-1}, can only increase by about a factor of three over its initial value of $(T/|W|)_{\rm init}\sim 0.09$, and only barely reaches the critical value of dynamical instability for bar formation $(T/|W|)_{\rm dyn}\sim 0.27$. It is therefore not surprising that we do not see a dynamical growth of nonaxisymmetric perturbations. We expect that these results hold for any moderately stiff equation of state, for which the corresponding critical configurations are similarly compact.

The study reported here focuses on *uniformly* rotating neutron stars, for which we adopt a moderately *stiff* equation of state and consider a configuration which is moderately compact initially $(R/M_g\sim 6)$. We speculate that for two alternative scenarios the results may be quite different, even qualitatively, both as far as the formation of a disk and the

growth of nonaxisymmetric perturbations are concerned.

For *differentially* rotating neutron stars, which are the likely outcome of the merger of binary neutron stars [4], $T/|W|$ may take larger values than for rigidly rotating neutron stars. It is therefore possible that such stars might develop dynamical bar mode instabilities.

Rotating supermassive stars (with masses $M \gtrsim 10^5 M_\odot$) or massive stars on the verge of supernova collapse are subject to the same dynamical instabilities, but are characterized by very *soft* equations of state ($\Gamma \sim 4/3$) and initial configurations which are nearly Newtonian (see [7,38]). Such stars therefore reach the critical value $(T/|W|)_{\rm dyn}$ for bar mode formation far outside the horizon radius. Moreover, R/M is very large initially, so that a disk may easily form (compare the discussion in [38]).

We will treat the collapse of both differentially rotating neutron stars and supermassive stars in future papers.

ACKNOWLEDGMENTS

Numerical computations were performed on the FACOM VPP 300R and VX/4R machines in the data processing center of the National Astronomical Observatory of Japan. This work was supported by NSF Grants AST 96-18524 and PHY 99-02833 and NASA Grant NAG5-7152 at the University of Illinois. M.S. gratefully acknowledges support by Grant-in-Aid (Nos. 08NP0801 and 09740336) of the Japanese Ministry of Education, Science, Sports and Culture, and JSPS.

[1] G. Cook, S. L. Shapiro, and S. A. Teukolsky, Astrophys. J. **398**, 203 (1992); **424**, 823 (1994).
[2] G. Cook, S. L. Shapiro, and S. A. Teukolsky, Astrophys. J. **422**, 227 (1994).
[3] G. Cook, S. L. Shapiro, and S. A. Teukolsky, Astrophys. J. Lett. **423**, L117 (1994).
[4] T. W. Baumgarte, S. L. Shapiro, and M. Shibata, Astrophys. J. Lett. **528**, L29 (2000).
[5] S. Chandrasekhar, Astrophys. J. **140**, 417 (1964).
[6] C. W. Misner, K. S. Thorne, and J. A. Wheeler, *Gravitation* (Freeman, San Franciso, 1973), Sec. 26.
[7] S. L. Shapiro and S. A. Teukolsky, *Black Holes, White Dwarfs, and Neutron Stars* (Wiley Interscience, New York, 1983).
[8] S. Chandrasekhar and J. L. Friedman, Astrophys. J. **175**, 395 (1972); **176**, 745 (1972); **177**, 745 (1972).
[9] B. F. Schutz, Astrophys. J., Suppl. **24**, 343 (1972).
[10] J. L. Friedman, J. R. Ipser, and R. D. Sorkin, Astrophys. J. **325**, 722 (1988).
[11] See N. Stergioulas, Living Reviews **1**, (8) (1998) for an historical review.
[12] M. Vietri and L. Stella, Astrophys. J. Lett. **507**, L45 (1998).
[13] T. Nakamura, Prog. Theor. Phys. **65**, 1876 (1981); **70**, 1144 (1983).
[14] R. F. Stark and T. Piran, Phys. Rev. Lett. **55**, 891 (1985); in *Dynamical Spacetimes and Numerical Relativity*, edited by J. M. Centrella (Cambridge University Press, Cambridge, England, 1986), p. 40.
[15] J. L. Friedman, J. R. Ipser, and L. Parker, Astrophys. J. **304**, 115 (1986).
[16] H. Komatsu, Y. Eriguchi, and I. Hachisu, Mon. Not. R. Astron. Soc. **237**, 355 (1989).
[17] M. Salgado, S. Bonazzola, E. Gourgoulhon, and P. Haensel, Astron. Astrophys. **291**, 155 (1994).
[18] K. Oohara and T. Nakamura, in *Relativistic Gravitation and Gravitational Radiation*, edited by J.-P. Lasota and J.-A. Marck (Cambridge University Press, Cambridge, England, 1997).
[19] M. Shibata and T. Nakamura, Phys. Rev. D **52**, 5428 (1995).
[20] The Binary Black Hole Grand Challenge Alliance, R. Gomez *et al.*, Phys. Rev. Lett. **80**, 3915 (1998).
[21] The Binary Black Hole Grand Challenge Alliance, A. M. Abrahams *et al.*, Phys. Rev. Lett. **80**, 1812 (1998).
[22] T. W. Baumgarte and S. L. Shapiro, Phys. Rev. D **59**, 024007 (1999).
[23] J. A. Font, M. Miller, W.-M. Suen, and M. Tobias, Phys. Rev. D (to be published), gr-qc/9811015.
[24] M. Shibata, Prog. Theor. Phys. **101**, 1199 (1999).
[25] M. Shibata, Phys. Rev. D **60**, 104052 (1999).
[26] S. Chandrasekhar, *Ellipsoidal Figures of Equilibrium* (Yale University Press, New Haven, CT, 1969).
[27] D. Lai and S. L. Shapiro, Astrophys. J. **442**, 259 (1995).
[28] J. L. Houser and J. M. Centrella, Phys. Rev. D **54**, 7278 (1996).
[29] For example, G. E. Brown and H. A. Bethe, Astrophys. J. **423**, 659 (1994).
[30] N. K. Glendenning, *Compact Stars* (Springer, New York, 1996).
[31] B. J. van Leer, J. Comput. Phys. **23**, 276 (1977).
[32] M. Shibata, Phys. Rev. D **55**, 2002 (1997).
[33] G. B. Cook, S. L. Shapiro, and S. A. Teukolsky, Phys. Rev. D **53**, 5533 (1996).
[34] Throughout this paper, we use ρ_c as the central rest mass density of equilibrium stars (initial data for our computation) and $\rho(r=0)$ as the central rest mass density of dynamically evolved stars (i.e., the latter changes during the evolution).
[35] Note that we recompute the constraint equations whenever we modify the initial equilibrium configurations (e.g., by depleting the pressure or by modifying the initial density profile).
[36] E. Seidel and W.-M. Suen, Phys. Rev. Lett. **69**, 1845 (1992).
[37] N. Stergioulas and J. L. Friedman, Astrophys. J. **492**, 301 (1998); S. Yoshida and Y. Eriguchi, *ibid.* **438**, 830 (1995).
[38] T. W. Baumgarte and S. L. Shapiro, Astrophys. J. **526**, 941 (1999).